Ceramics International 49 (2023) 21892–21902

Contents lists available at ScienceDirect

Ceramics International

journal homepage: www.elsevier.com/locate/ceramint

Structural properties of volcanic precursors-based geopolymers before and after natural weathering

Roberta Occhipinti [a], Maria Cristina Caggiani [a,*], Lavinia de Ferri [b], Zhuo Xu [c], Calin Constantin Steindal [b], Nima Razavi [c], Fabrizio Andriulo [b], Paolo Mazzoleni [a], Germana Barone [a]

[a] Department of Biological, Geological and Environmental Science, University of Catania, Italy
[b] Department of Collection Management-Museum of Cultural History, University of Oslo, Norway
[c] Department of Mechanical and Industrial Engineering, Norwegian University of Science and Technology, Norway

ARTICLE INFO

Handling Editor: Dr P. Vincenzini

Keywords:
Geopolymers
Natural weathering
Durability
Structural properties

ABSTRACT

The structural properties of geopolymers based on locally available volcanic feedstocks were here investigated in the optics of the development of sustainable non-structural building materials. Geopolymer binders and mortars based on two volcanic pyroclastic residues from Mt. Etna (ejected ash and a paleosoil, named "ghiara") were studied to assess the effects of natural weathering.

The strength and durability of the resultant products were examined before and after six months of outdoor exposure by comparing ultrasound pulse velocity (UPV), specific weight, Brazilian Disk test (BD) and Digital Image Correlation (DIC) together with Dynamic Vapour Sorption (DVS) results. DVS data were also compared to those of pure salts (e.g. sulphates and carbonates) commonly occurring in geopolymers as efflorescences.

The results obtained on unexposed and exposed samples and the relationship between the moisture transportation, efflorescence development, and structure degradation have shown a better response of the volcanic ash-based geopolymers to weathering in the hot summer Mediterranean climate zone than ghiara-based products. The latter are more affected by exposure conditions as revealed by the decrease of UPV, the influence of efflorescences on moisture adsorption-desorption curves and the consequent worsening of mechanical performances.

The correlation between UPV and DVS applied for the first time to the study of volcanic precursors-based geopolymers exposed to natural weathering has proven to be an effective and useful tool for assessing the durability of materials.

1. Introduction

Low carbon cements, i.e. geopolymers (GP) have been an object of research as an alternative solution for the cement industry [1,2]. Ordinary Portland Cement (OPC), globally used for construction, significantly contributes to the greenhouse gases emission due to the high energy consumption required for clinker calcination (usually at 1400–1450 °C) and grinding of raw materials, coal, and clinker. Moreover, cultural heritage is a field in which geopolymers may actually find application [3–8], since their chemical, physical and mechanical properties can be modified and tailored to meet the requirements of restoration good practices.

Geopolymers are inorganic materials obtained by mixing an aluminosilicate powder of natural or synthetic origin, with an alkaline activator (e.g., sodium hydroxides and/or sodium silicate solutions). When Si and Al contents are properly balanced with the cations in the alkaline solutions, the reaction takes place, and a geopolymer product is obtained at room temperature. A complete and detailed description of the state of the art related to these materials and recent developments can be found in Refs. [9–11]. The possibility to employ various industrial wastes as raw materials (e.g., fly ash metallurgical slags [12], glass wastes [13] and residues of mining activities [14]) besides natural ones, makes them even more suitable in the perspective of green materials development. However, the nature and concentration of activating solution, the water content, the binder composition, and the curing temperature (i.e., the whole mix design) influence the geopolymers

* Corresponding author. Corso Italia, 57, 95129, Catania, Italy.
E-mail address: mariacristina.caggiani@unict.it (M.C. Caggiani).

https://doi.org/10.1016/j.ceramint.2023.04.013
Received 21 February 2023; Received in revised form 30 March 2023; Accepted 4 April 2023
Available online 5 April 2023
0272-8842/© 2023 The Authors. Published by Elsevier Ltd. This is an open access article under the CC BY-NC-ND license (http://creativecommons.org/licenses/by-nc-nd/4.0/).

properties, which therefore must be carefully evaluated. Thus, the possibility of exploiting a variety of aluminosilicates as precursors, together with the opportunity of generating products with specific desired properties, makes geopolymers versatile for a wide range of applications and adaptable to different geographic areas.

The question of whether geopolymer materials are durable, thus resisting high temperatures, abrasion, chloride intrusion and wetting–-drying cycles, remains the major obstacle to meet the standard requirements for structural purposes and hence to their commercial adoption. Although some studies [15] reported that geopolymers have excellent chemical and physical properties, such as weathering, abrasion resistance and chemical stability, most papers [16–19] describing the mechanical properties of geopolymers do not investigate their durability characteristics. Therefore, deepening the knowledge on this aspect is vital to achieve materials with a higher resistance against external agents, thus guaranteeing a longer service life.

In general, the durability of concrete structures is related to the capacity of the material to avoid the penetration of aggressive agents (sulphates, chlorides, CO_2 …) in its porous structure, and its resistance is influenced by its properties of transfer (porosity, permeability and diffusivity) [20]. The variability in terms of particle sizes and morphologies, due to the use of different precursors, aggregates, and crystalline phases, often makes geopolymers heterogeneous. This determines their anisotropy, which can also be influenced by the formation of cracks, fractures, pores, etc. during the curing period. The understanding of the mechanical and crack behaviours, therefore, is critical and necessary for their applications. An optimal employment of additives or aggregates can minimize the porosity and maximize the binding effect of geopolymer concretes, protecting them from damage due to the environmental exposure.

Ultrasound pulse velocity (UPV) allows to estimate the elastic properties [21] and to detect fracture and cracks [22] by measuring the velocity and the attenuation of the ultrasonic waves in a given frequency band.

The basic theory of ultrasonic wave propagation in concrete has been described in detail by Jones [23]. It is known that the velocity of waves in concrete is influenced by the same properties that determine its elastic stiffness and mechanical properties [24], i.e. the elastic properties and the density of the concrete [25], and can be influenced by changes in the material structure such as the propagation of cracks.

In the literature, UPV has been applied to assess damages due to cracking in strength tests of concrete specimens, such as compression tests [26] and tensile tests [27], as well as of geopolymers materials [28]. Moreover, UPV variations have been frequently used in the assessment of continuous damaging processes in concrete and other cement-based materials [29] and building stones [30], in order to identify the mechanism associated with the value of tensile strength.

The tensile fracture is an important failure mode describing the critical states of stresses or energy near the crack tip required for the initiation of brittle fracture. Some authors [31,32] state that failure in Brazilian disks starts from a point directly under the loading point due to the presence of largest equivalent stress at the loading point of the end surface. On the contrary, several other research studies have concluded that the tensile strength resulting from Brazilian disc tests appear to give a reasonable value for tensile strength of rock-like materials [33–36]. Regardless, this technique has been widely used by the researchers in the field to obtain an indication of tensile properties of rocks, concretes and geopolymers, despite the use of a different terminology [37–39]. Some optical non-contact techniques can provide full-field deformation information, which is the complete set of deformation value across an entire surface or region of interest rather than just a single point or location, such as digital image correlation (DIC) method. DIC is a non-contact, full-field and high-resolution method that provides accurate and detailed information about the deformation behaviour of materials and structures under various loading conditions. It is one of the most powerful optical full-field measurement methods and has been applied in various fields in the past decades [40–42].

In addition, and in combination to fracture propagation and transfer properties, efflorescences occurrence must be considered among the factors that can severely influence the durability of geopolymers in terms of structural degradation, due to the high availability of OH^- and Na^+ ions in the highly alkaline geopolymer environment. Efflorescences of sodium carbonates are often found in pores of alkaline building materials due to the reaction of sodium compounds with environmental CO_2 [43]. Their presence has been already reported for geopolymers as well [44,45] and can induce structural degradation as shown by Ref. [46], disclosing the relationship between the alkali leaching due to the surface crystallization of carbonates and strength reduction [46]. The wetting or drying conditions geopolymers are exposed to, play a dominant role in controlling the moisture absorption/desorption isotherms, which can be studied through Dynamic Vapour Sorption (DVS). The sorption (-desorption) isotherms define the relationship between the concentration of a mass in a porous material isothermally in equilibrium with that in the environment. For water, the relation is defined between the moisture content in the material and the relative humidity (RH%) of the surrounding environment at equilibrium and constant temperature [47]. The total sorption plot includes curves for both the adsorption and the desorption processes because of the strong influence of the history of wetting and drying of the specimen [47]. Hygroscopic materials exhibit different sorption isotherm depending on their microstructure and on the interactions with the adsorbate, i.e. moisture [48]. Among the six types of isotherms reported by the International Union of Pure and Applied Chemistry (IUPAC), type III is generated by materials with very weak interactions with the adsorbate and is characterised by a concave shape over the entire RH% range. In parallel, in type II curves the inflection point indicates the transition from mono to multilayer adsorption or from multi to monolayer desorption [48].

To the best of the authors knowledge, there are no studies in the literature relating DVS and UPV results, thus the unique contribution of this study is to provide a detailed correlation of the results of these techniques.

In previous works [8,49,50], Sicilian volcanic precursors (ash, a volcanic paleosoil called “ghiara”, and pumice) were used together with metakaolin for preparing geopolymers.

In particular, volcanic ash and ghiara based geopolymers have shown excellent results in terms of geopolymerisation reaction, mechanical and chemical properties. However, the durability of these materials, which needs to be guaranteed both in construction and restoration field, has not been studied in depth yet.

Following a previous work [51], in which preliminary results concerning the effect of weathering on alkali activated volcanic ash, ghiara binders and mortars were presented, new data are here reported and discussed. This work provides a comprehensive understanding of their structural properties before and after the atmospheric exposure by means of UPV, along with disclosing the relationship between the materials’ structure and their mechanical properties, studied through the Brazilian Disk test (BD) and DIC analysis.

DVS data were reconsidered and compared to the results obtained with pure sulphates and carbonates, that can occur on geopolymers as efflorescence.

A thorough understanding of the relationship between the moisture transportation, efflorescence development, and structure degradation is a key requirement to predict the durability of geopolymers, especially for the products used for field applications, such as the building and restoration sector, in the frame of research for sustainable construction materials and energy saving.

2. Experimental

2.1. Materials

Based on previous formulations [50,52], volcanic ash and ghiara

from Mt. Etna (Sicily) and metakaolin (MK, ARGICAL™ M − 1000, Imerys, France) were used as solid precursors. Ghiara is a red volcanic paleosoil found beneath solidified lava flows whose deposits are probably widespread around the world [53,54].

8 M sodium hydroxide solution (provided by Carlo Erba reagents s.r.l., Italy) and sodium silicate (molar ratio $SiO_2/Na_2O = 3.3$, supplied by Ingessil s.r.l., Italy) were the liquid activators.

Volcanic ash and ghiara with particles size <2 mm were selected and dry milled to obtain a grain-size fraction <75 μm. MK was added to the raw materials and mixed by hand to homogenise the solids. Binders (labelled GM20B- VM20B) were prepared by mixing the solids with the alkaline solution. The pastes were mixed for 5 min by using a mechanical mixer.

Mortars (labelled GM20M-VM20M) were prepared by adding aggregates to the binders. Sizes and proportions of the aggregates added to binders for mortars preparation were as follows: 32.5% (2< Ø < 1 mm); 31.5% (1.0 < Ø < 0.5 mm); 29% (0.5 < Ø < 0.125 mm); 6% (0.125 < Ø < 0.075 mm); 1% (Ø <0.075 mm). For each formulation, the ratio between liquid (alkaline solutions) and solid components (ash/ghiara and MK) (L/S, by weight) was chosen to obtain adequate workability of the slurry and for casting it in the moulds [51]. Table 1 reports the synthesis parameter of binders and mortars. Six prisms 20 × 20 × 80 mm and six disks (Ø = 45 mm, and thickness varying from 20 to 25 mm) were prepared for each formulation of binders and mortars (Fig. 1a and b). All samples have been cured at 25 ± 3 °C for 28 days. Three replicas of each sample were tested after curing, while the other three were exposed to the atmospheric environment for six months [51] and tested after the exposure.

In addition to the geopolymers, the vapour sorption and desorption of a selection of reference salts were assessed by DVS. Salts were chosen based on the results of previous spectroscopic analysis published in a former study [51] assessing the presence of sodium carbonates for the studied formulations. Specifically, Na_2CO_3, $Na_2CO_3{\cdot}10H_2O$ and $Na_3H(CO_3)_2{\cdot}2H_2O$ were identified on both the core and the surface of specimens. In addition, several salts commonly reported as weathering products on geopolymers, traditional mortars and concrete [14,55] ($CaCO_3$, $CaSO_4{\cdot}2H_2O$, Na_2SO_4 and $Na_2SO_4{\cdot}10H_2O$) were tested. The materials subjected to the DVS analysis were: $CaCO_3$ (pro analysis, MERCK), Na_2CO_3 (EMSURE®ISO analytical degree, Supelco), $Na_2CO_3{\cdot}10H_2O$ (99+%, Alfa Aesar), $Na_3H(CO_3)_2{\cdot}2H_2O$ (natural crystal), and calcium and sodium sulphates: $CaSO_4{\cdot}2H_2O$, Na_2SO_4 (Carlo Erba, assay ≥99%), $Na_2SO_4{\cdot}10H_2O$ (Carlo Erba, assay ≥99%).

2.2. Methods

In this study, ultrasonic pulse velocity (UPV), Brazilian Disk test (BD) with Digital Image Correlation (DIC) analysis, and Dynamic Vapour Sorption tests (DVS) tests were carried out on the described volcanic-based alkali activated binders and mortars before and after the atmospheric exposure described in Ref. [51] (Fig. 1).

2.2.1. Ultrasound pulse velocity

Measurements of the speed of a pulse of ultrasonic longitudinal stress waves were performed in transmission mode using a field instrument PUNDIT Plus (Portable Ultrasonic Nondestructive Digital Indicating Tester), manufactured by CNS Farnell, UK (Fig. 1c). The instrument had a resolution of 0.1 μs. A pair of 200 KHz single-frequency transducers, sending a 1200 V pulse, were used in direct contact with the sample using an aqualene low attenuation dry couplant (2 mm thick) as a coupling agent, and a slight pressure to ensure good contact between the transducers and the sample surface. Plexiglas and brass were used to calibrate the set-up. The time-of-flight (ToF) was corrected with the time it took the pulse to travel through the set-up with no sample. Ultrasound measurements were taken for each sample type, on three replicate prisms (20 × 20 × 40 mm) [56]. Measurements were performed three times in each direction, i.e. long (L) and short (S) axes switching between the sample faces.

2.2.2. Brazilian test

Tensile properties of the studied geopolymers were analysed by performing compressive mechanical testing on Brazilian Disk (BD) specimens. The testing setup for mechanical testing of BD specimens is represented in Fig. 1d. The specimens were tested using an Instron 8850 servo-hydraulic test machine (Massachusetts, United States) with a load cell capacity of 250 kN at a constant displacement rate of 0.2 mm/min. The test results in form of load-displacement data were then extracted from the testing program. Digital Image Correlation (DIC) method was used for direct measurement of the displacement field on the front face of the BD specimens. This method is a suitable option for full-field measurement of displacement and strains and its principals work by tracing the movement of specific points on the surface of the test specimen. For this aim, the front face of BD specimens was spray painted in matt white to create a uniform background for the main black points which were painted on top of the white paint. Sequential photos with shooting interval of 0.2 s were taken during the test by use of a high-performance digital camera (Stingray F504B-Allied Vision, Germany) during the experiment and were used as the input data for DIC software (VIC-2D, United States).

2.2.3. Dynamic vapour sorption tests

To quantify the tendency of samples to retain water vapours and to measure sorption and desorption dynamics, DVS analyses were carried out on an automated multi-sample moisture sorption analyser Vsorp Enhanced (ProUmid, Germany-Ulm) (Fig. 1e). Solid specimens of geopolymers (~70 mg cubes) previously conditioned at 25 °C and 5% RH for 60 h, were tested under isothermal conditions (25 ± 0.1 °C). SRH was dynamically changed in 9 steps of 10% each covering a range from 5 up to 95%. The mass criterion to proceed to the next RH step (equilibrium condition) was considered to be reached when the weight samples changed by less than $dm/dt < 0.002$ wt% over four weight measurements within a time interval of 60 min; if the equilibrium was not reached for all the samples within 60 h, the apparatus proceeded to the next RH step.

Measurements on salts were performed in the same dm/dt and time conditions. However, due to the presence of deliquescent salts, a default weight limit increase of 1000% within the RH interval 10–95% was used. The considered RH interval was 90–95% RH. Two and three replicates were tested for each geopolymer composition and salt, respectively.

Table 1
Details of samples preparation.

Sample	Label	Solid precursors (wt. proportion)	Na_2SiO_3/NaOH (wt. ratio)	Aggregate wt.% on the slurry	Liquid/Solid* (wt. ratio)
Volcanic ash/metakaolin binder	VM20B	80/20	1.7	0	0.32
Ghiara/metakaolin binder	GM20B	80/20	1.7	0	0.32
Volcanic ash/metakaolin mortar	VM20M	80/20	1.7	30	0.32
Ghiara/metakaolin mortar	GM20M	80/20	1.7	30	0.38

Letter w (weathered) was added to the labels to indicate the samples after exposure. *Liquid/solid ratio is referred to the whole alkaline solution to solid precursors ratio.

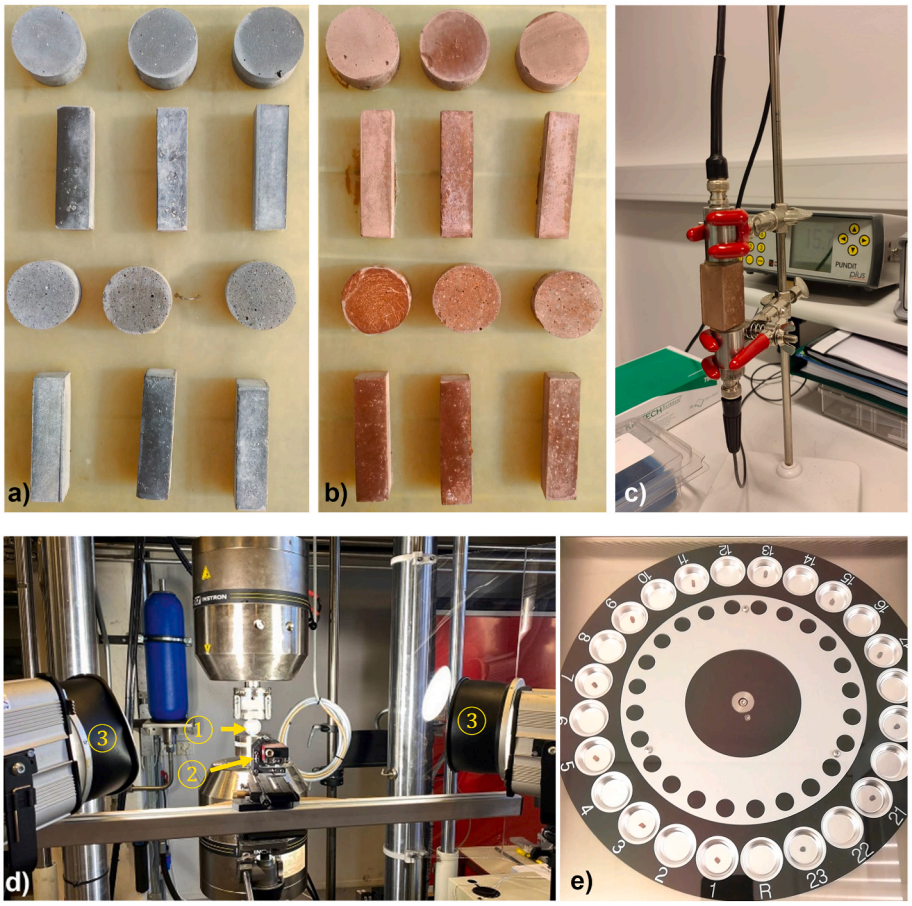

Fig. 1. Volcanic ash- (a) and ghiara- (b) based geopolymer binders and mortars after weathering; ultrasound pulse velocity (c), Brazilian disk testing, (1): loading geometry of Brazilian disk specimen, (2): DIC camera, (3) lights (d) and dynamic vapour sorption (e) setups.

3. Results

3.1. Ultrasound pulse velocity (UPV) and specific weight

Ultrasound pulse velocity test results are shown in Table 2 and Fig. 2. Flexural and compressive strength data from Ref. [51] are also reported for comparison in Fig. 2. The lowest UPV values were generally registered in case of volcanic ash-based unexposed samples (VM), while for the ghiara-based unexposed ones (GM) higher values were recorded. Moreover, the addition of the aggregates seemed to lead to an increase of the velocity values for both types of samples, VM and GM.

After the outdoor exposure, the two sets of samples showed different behaviours. While the ultrasound velocities of volcanic ash-based geopolymers tend to show higher values than the fresh samples (VM20B and VM20M vs. VM20Bw and VM20Mw), the ghiara-based ones have an opposite behaviour: the unexposed binders and mortars showed higher values of the velocity than the exposed ones (GM20B and GM20M vs. GM20Bw and GM20Mw) (Table 2, Fig. 2).

Moreover, for both groups (VM and GM), fresh and weathered, differences in UPV measured along the two axes (S and L) were observed. Published studies reported that given the inhomogeneous nature of concrete, variations were recorded when measuring UPV through shorter versus longer paths, due to the attenuation caused by the anisotropy of the cement: voids, cracks, and aggregate grains [57].

Additionally, in both ghiara and volcanic ash series, the relationships between the average values of UPV are consistent with those of the respective flexural and compressive strength data (Fig. 2).

Specific weights of the specimens were determined by calculating the ratio between the dry weight and the volume of each semi-prism specimen. The average values (three measurements per sample) are reported in Table 2. Overall, the unit weights of the weathered specimens, either binders or mortars, are lower than those of the unexposed ones although the differences are not significant for volcanic ash-based ones (Table 2).

Table 2
Ultrasound wave velocity values (m/s) measured along the two directions, S (average of the measures on the two short axes) and L (long axis), together with specific weight (g/cm^3) calculated for each sample and relative standard deviation (σ).

	Average Velocity [m/s]				Average Specific gravity [g/cm^3]	
Sample	S	σ	L	σ		σ
GM20B	2431	21	2885	12	1.88	0.024
GM20Bw	2335	14	2681	7	1.82	0.010
GM20M	2470	11	2869	18	2.00	0.007
GM20Mw	2398	16	2759	13	1.94	0.023
VM20B	2247	19	2592	12	1.85	0.025
VM20Bw	2415	27	2705	17	1.84	0.039
VM20M	2367	16	2669	10	1.97	0.010
VM20Mw	2487	24	2833	20	1.94	0.026

3.2. Brazilian Disk test (BD) and digital image correlation (DIC)

The peak load values for all the samples are shown in Table 3. Since the tested specimens varied in thickness, the suggested formulation in ASTM D3967 for calculation of splitting tensile strength was used to obtain the peak stress. Based on ASTM standard, the splitting tensile strength of Brazilian Disks can be calculated as:

$$\sigma_t = 2P/\pi LD \qquad \text{Equation (1)}$$

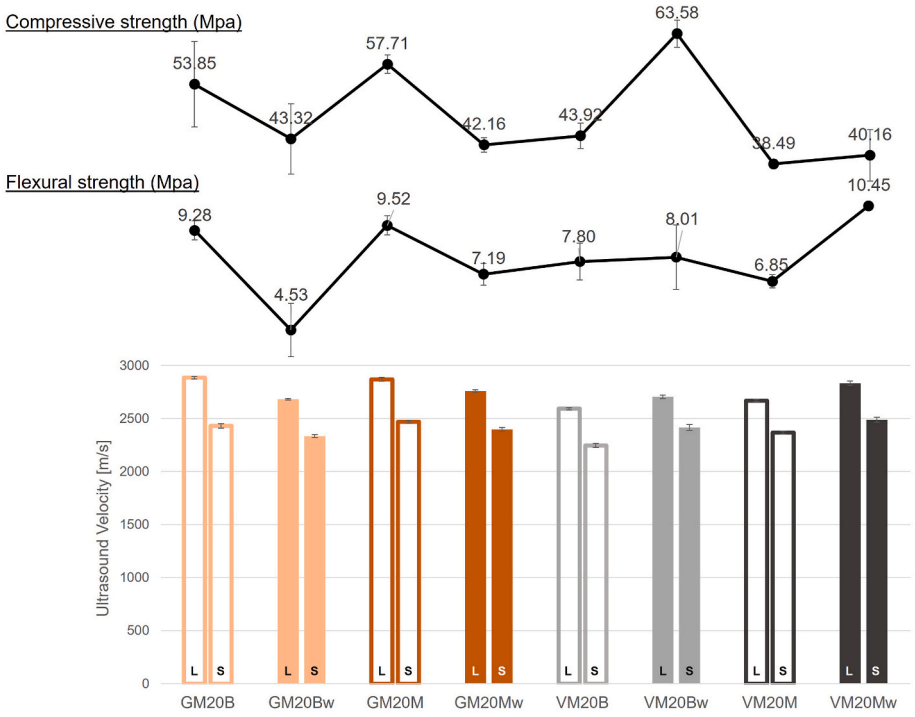

Fig. 2. Ultrasound pulse velocity results along the short (S) and long (L) axis for binders (GM20B and VM20B) and mortars (GM20M and VM20M) before and after (label w) environmental exposure. Compressive and flexural strength data from Ref. [51] are reported for comparison.

Table 3
Mechanical properties of the tested geopolymers (average and STD).

Sample	GM20B	GM20Bw	GM20M	GM20Mw	VM20B	VM20Bw	VM20M	VM20Mw
Thickness[a] (mm)	22.99 (±3.01)	23.13 (±0.97)	22.63 (±2.55)	24.50 (±0.26)	18.53 (±2.79)	23.91 (±0.45)	18.75 (±2.12)	23.54 (±1.04)
Peak load (kN)	14.34 (±2.84)	9.17 (±1.48)	7.52 (±1.78)	6.52 (±1.99)	10.75 (±2.60)	11.36 (±0.85)	9.36 (±1.51)	8.87 (±1.15)
Peak stress, σ_t (MPa)	8.79 (±0.60)	5.64 (±1.09)	4.67 (±0.59)	3.76 (±1.14)	8.15 (±0.76)	6.73 (±0.61)	7.04 (±0.34)	5.34 (±0.73)

[a] Measured thickness at the centre of the test specimen.

in which σ_t is splitting tensile strength of the tested material, P is the maximum applied load during the test, and L and D are the thickness and diameter of the Brazilian Disk specimen, respectively.

The comparison of the peak load and peak stress values among the different groups of samples leads to the observation that ghiara binder performance worsens after exposure, in accordance with UPV and compressive and flexural strength (Fig. 2), and after addition of aggregates too. On the other hand, other comparisons are not significant due to the high error caused by the small number of replicates and their marked variability.

The horizontal strain contours on the front face of test specimens were analysed during the tests and the results for four intervals are presented in Fig. 3. In the last column of this figure, a picture of the tested specimen used for DIC analysis is presented. According to these observations, no significant difference in the fracture pattern of the test specimens after outdoor exposure was detected. Among the tested cases, ghiara based binder (GM20B) represented the most unstable crack propagation which resulted in shattered pieces of the specimen after the fracture. On the contrary, ghiara-based mortar showed a typical brittle fracture by splitting the test specimen in half. In this case, very limited crack branching could be observed. Both volcanic ash-based binder and mortar illustrated similar fracturing pattern with the crack appearing along or very close to the maximum tensile plane in the specimen.

Although the design of Brazilian disk is based on the start of the crack at the centre of the test specimens, localized strains near the contact points of the test specimens were observed in DIC images indicating that the start of the cracking may have been from these points. This was also reported in few research studies debating the validity of this type of test. For instance, Fairhurst [58] reported that failure in Brazilian disks can occur away from the centre of the specimen for small angles of loading contact area while testing materials that have low compression to tension strength ratios. In these cases, a lower tensile strength can be expected from Brazilian test than the true tensile strength of the material. Similar argument was also presented in Refs. [31,32]. It can here be observed that in most cases, the maximum horizontal strain appears at the vicinity of the contact area, extending toward the opposite side along the plane of maximum tensile stress. In the specific case of GM20Bw, however, this maximum strain is observed at the centre of the disk and far from the contact area. It should be reminded that this specimen represented the most unstable fracture among all cases.

3.3. Dynamic vapour sorption (DVS)

3.3.1. Geopolymer samples

The absorption-desorption isotherms of formulations listed in Table 1 have been collected in order to evaluate the behaviour of tested materials toward water vapours.

Curves obtained in the range 5–95% RH for binders and mortars, before and after exposure to the environment, are presented in Ref. [51]. Differences can be evaluated from the shape of the sorption curves: for both the unexposed and exposed samples, type II isotherms were obtained, as expected for mortars-like materials. However, for data obtained before exposure, sigmoids are particularly flattened at low RH%, making them almost resembling type III curves [48]. In this work, we

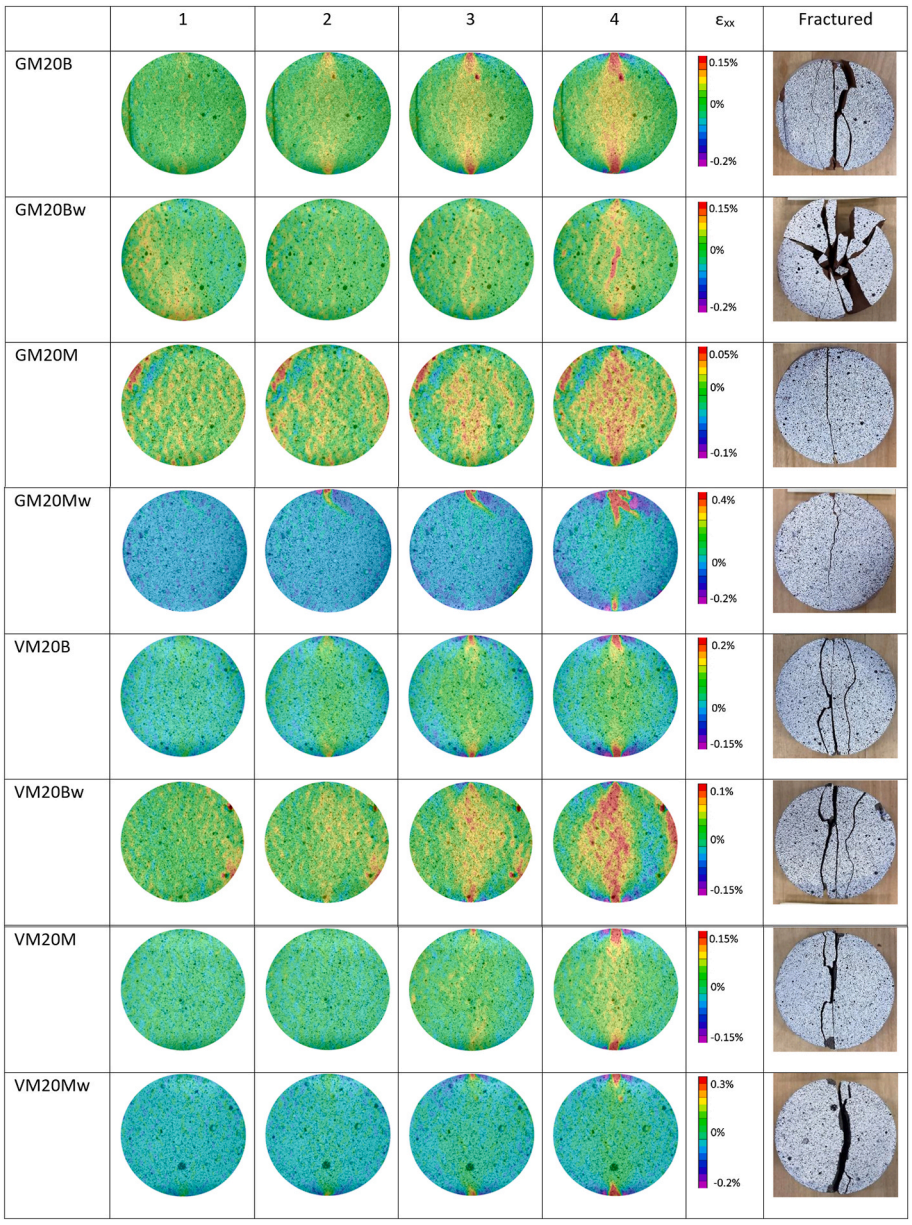

Fig. 3. Horizontal strain contours of the geopolymer Brazilian Disk specimens at four different intervals of the tests (numbers 1, 2, 3, 4 represent 0.11, 0.22, 0.33, and 0.44% global strain). (For interpretation of the references to colour in this figure legend, the reader is referred to the Web version of this article.)

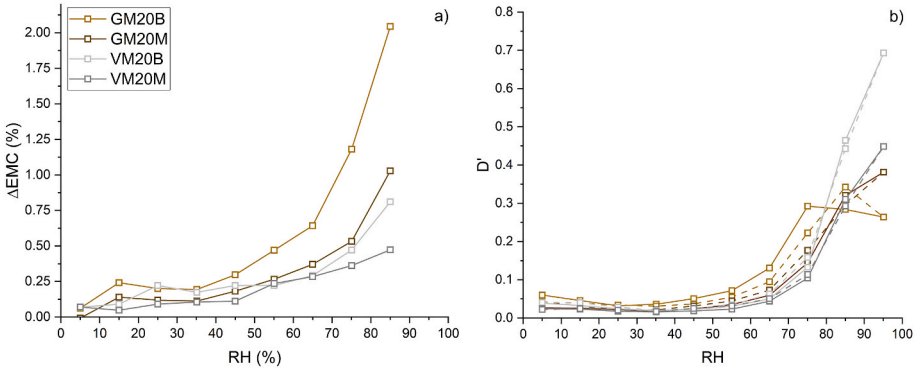

Fig. 4. Sorption-desorption hysteresis (a) and first derivative curves (b, solid lines-adsorption; dashed lines-desorption) of unexposed specimens with the composition listed in Table 1. Lines are guides for eyes. (For interpretation of the references to colour in this figure legend, the reader is referred to the Web version of this article.)

will deepen the understanding of the absorption-desorption process, with the study of the hysteresis and first derivative curves and the time vs. EMC/RH plots.

A separation of the sorption and desorption curves of each specimen is visible starting from RH% = 35–45 and it tends to reach its maximum around 85% RH. Such a difference is the so-called hysteresis (ECM_{des}-ECM_{ads}) (Fig. 4a) and, especially for GM compositions, it seems to be strongly affected by the presence of non-absorptive aggregates. On the other hand, the hysteresis of VM samples seems to be less affected by the introduction of aggregates in the mixture. Additionally, trona and natron efflorescences were attested on the fresh materials [51]. Trona ($Na_3H(CO_3)_2{\cdot}2H_2O$) is reported to be a very stable salt up to RH values < 90% [59,60] while natron ($Na_2CO_3{\cdot}10H_2O$) is a deliquescent salt for RH values higher than ~77% (see below).

In general, hysteresis is caused by diverse prevailing phenomena in different RH% intervals. In particular, it is possible to distinguish two intervals, below and above 35% RH, for curves shown in Fig. 4a. The moisture content difference at higher RH values (>35%) is usually attributed to the complex pore network in which pores of various sizes, normally present in concretes as well as in geopolymer-based materials, are interconnected to each other. An explanation for this behaviour has been given in relation to the "inkbottle" theory. During the adsorption process, water can have access to the entire pore network, but the portion condensed in the bigger voids is kept until the smaller channels connecting them to the surface are emptied. The higher the number of necks precluding the emptying of larger pore, the more the desorption process is affected [61,62]. As evident in Fig. 4a, this seems to be the prevailing phenomenon for all the tested specimens for RH values higher than 35–45% and the result is consistent with what reported in the literature [63].

Hysteresis at low RH (<35%) is due to the removal of interlayer water and possible structural collapses. This phenomenon is not completely reversible on rewetting, especially when the drying process occurs as a consequence of a strong temperature increase [63]. As shown in Fig. 4a, this part of the curves displays very low values indicating that the loss of interlayer water is not a dominant process.

As indicated above, for type II isotherms, the inflection point gives information about the transition from mono to multi layers and vice versa. For this reason, the first derivative of each curve was calculated, and results are shown in (Fig. 4b). In general, the first derivative helps in evaluating the rate at which EMC changes with RH and thus the tendency of the material to gain or release moisture. In the case of unexposed binders, both the adsorption and desorption processes are quite slow at RHs lower than 45%. On the other hand, when aggregates were added, this slow gain/release interval widened up to 65% RH. After this value, the processes get faster as indicated by the steep increase of the slopes of the curves. As evident, it is not possible to identify a maximum corresponding to an inflection point in the sorption-desorption isotherms, except for GM20B, at 75%.

However, for all the samples the curves invert between 80 and 85 RH %. This means that between 75% and 85% RH, all the materials tend to release moisture at a higher rate than for the sorption process.

More information about the behaviour of unexposed materials can be obtained from the EMC/time plots shown in Fig. 5a. As shown, starting from 65% RH it seems that both the water adsorption and desorption occurred gradually, with a certain stabilisation at 95% and 85% RH.

Fig. 6a reports the hysteresis curves obtained for the cured samples, whose values are of one order of magnitude lower than the unexposed ones. For all the exposed specimens, a first minimum is clearly visible at 25% RH and a second one at 65%, meaning that almost no difference exists between the sorption and desorption curves. Moreover, all the samples show the highest hysteresis value between 35 and 55% RH. Finally, a clear separation between binders and mortars was noticed again, confirming the behaviour already observed for the unexposed samples.

The derivative curves obtained for the exposed geopolymers are shown in Fig. 6b. The general trends for which we observe an increase in the speed of water sorption and desorption of RH values higher than 75% remains. Furthermore, all the desorption profiles (dashed lines) show a negative slope between 35 and 45% RH, and a maximum between 25 and 35% RH, the interval corresponding to the transition from the multi to the monolayer. In addition, between 15 and 45% RH, the derivative of the desorption curves of binders and mortars tend to separate in the same way observed for high RH values, i.e., binders show higher values than mortars. As evident from Fig. 6b, it is not possible to clearly distinguish a maximum in the first derivative of the sorption curve (solid lines).

Finally, curves of Fig. 5b allow noticing how differently the cured materials reacted when exposed to water moisture compared to the fresh samples. All the recorded profiles show a peak appearing between ca. 180 and 210 h and corresponding to the transition between 85 and 95% RH. It may indicate the occurrence of a transition/crystallization process, specifically from an amorphous into a crystalline status. This could also explain the successive mass drop [64].

3.3.2. Reference salts

As reported in Ref. [51], sodium carbonates were found by FTIR spectroscopy on both unexposed and exposed samples. Particularly, Natron ($Na_2CO_3{\cdot}10H_2O$) and trona ($Na_3H(CO_3)_2{\cdot}2H_2O$) were detected on the unexposed materials, while natrite (Na_2CO_3) was observed on the exposed ones. To assess their influence and of other potential detrimental products (specifically of sulphates), sorption-desorption isotherms were collected and results are shown in Fig. 7a. As expected, gypsum ($CaSO_4{\cdot}2H_2O$) and calcite ($CaCO_3$) do not display a significant adsorption curve, a moderate gain is shown for Na_2SO_4 and $Na_2SO_4{\cdot}10H_2O$ starting from 70% RH, while natron and natrite tend to adsorb a relevant amount of water after 60% RH. As anticipated above, at 25 °C natron and natrite are reported to be deliquescent at RH values

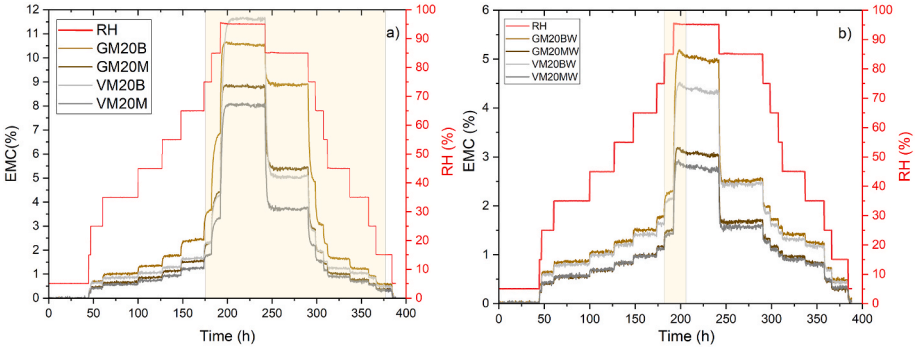

Fig. 5. Plots showing the change of ECM (%) and RH (%) over Time (h) for the unexposed (a) and exposed (b) samples. (For interpretation of the references to colour in this figure legend, the reader is referred to the Web version of this article.)

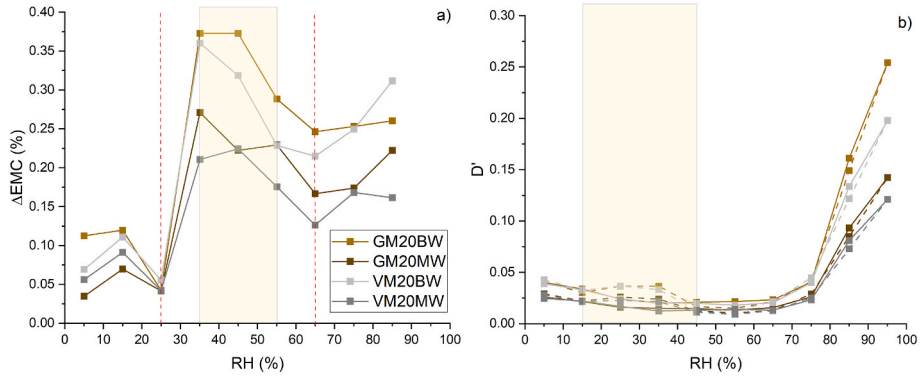

Fig. 6. Sorption-desorption hysteresis (a) and first derivative curves (b, solid lines-adsorption; dashed lines-desorption) of cured specimens whose composition is listed in Table 1. Lines are guides for eyes. Yellow areas define RH intervals discussed in the text. (For interpretation of the references to colour in this figure legend, the reader is referred to the Web version of this article.)

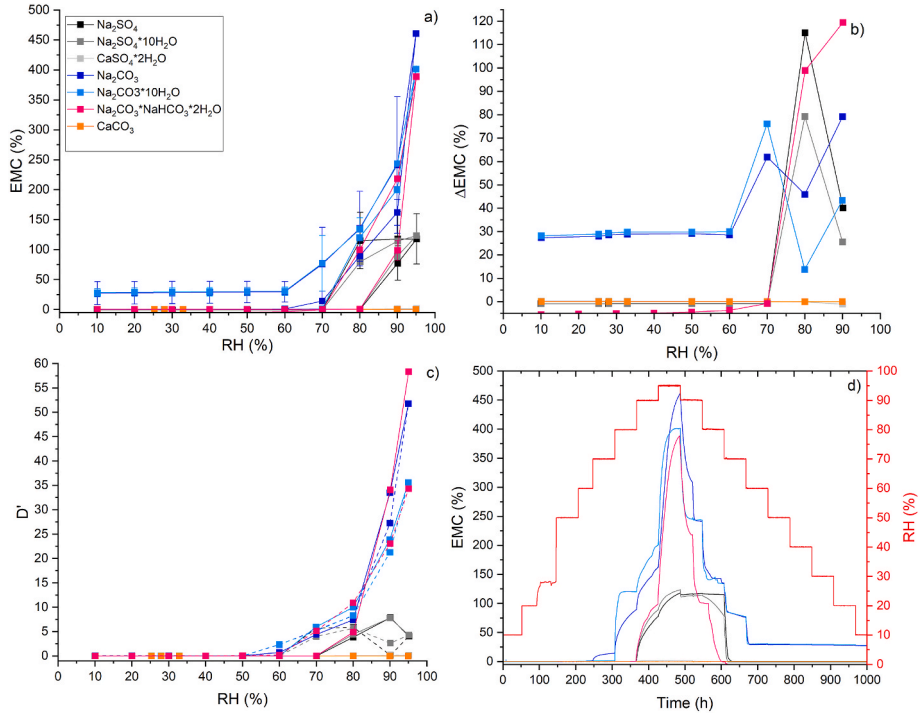

Fig. 7. Sorption-desorption isotherms (a), hysteresis (b), first derivative curves (c, solid lines-adsorption, dashed lines-desorption), and plots showing the change of ECM and RH over Time (d) of salt references. In a, b, and c lines are guides for eyes. (For interpretation of the references to colour in this figure legend, the reader is referred to the Web version of this article.)

higher than 77% and 88.2%, respectively [43]. Changes are confirmed by the hysteresis values (Fig. 7b): while no modifications are observable for gypsum and $CaCO_3$, the curves of the two sodium sulphates reach the maximum difference at 80% RH. Consequently, between 70 and 95% RH these two salts tend to adsorb and then lose a quite high amount of water vapours without any permanent modification of their structures. In parallel, for natrite and natron the hysteresis values never decrease below 30% RH due to the adsorption of water molecules that remain in the material until the end of the process leading to a structural modification of the network. For both the sodium carbonates, the hysteresis shows the same behaviour with a first maximum at 70% RH and, second one at 90% RH and a minimum in between.

When looking at the first derivatives of the isotherms (Fig. 7c), a change in the speed at which sorption and desorption occur is particularly evident for $Na_2SO_4{\cdot}10H_2O$ between 60 and 80%RH, with the desorption process taking place slower. On the other hand, the release of water moisture by natron and nitrite seems to be faster than the sorption, and this is particularly evident in Fig. 7d, showing the variation of EMC (%) and RH% over time. In most of the cases, recorded mass changes do not strictly correspond to a change in the RH% conditions, meaning that the studied deliquescent salts, did not reach the equilibrium in the predetermined time interval, kept as a constant setting for both the experiments on geopolymers and salts in order to obtain comparable results. Finally, a (phase/structural) change occurs during the desorption cycle of natron and natrite between 550 and 600 h, corresponding to 90-80% RH.

4. Discussions

The relationship between ultrasonic pulse velocity, specific weight, mechanical strength, and moisture sorption behaviour before and after outdoor exposure is discussed in the following.

It is well-known that UPV is influenced by several properties inducing heterogeneity in the material, including aggregates, age, moisture content, microcracking, porosity and/or diverse structure of the matrix (amorphous, crystalline) [26,65–67]. Ultrasonic waves travel faster through solid media than through liquid and gas. So, as well as in concrete, also in geopolymers the UPV depends on density and elastic properties of the material [68].

If we compare the results obtained on the different groups of products, the addition of aggregates to binders does not significantly affect the specific weight values. However, the values of the velocities recorded an increase with the addition of the aggregates that could be explained by an increase in heterogeneity.

Considering, instead, the effect of weathering on geopolymers, the UPV values are in accordance with the flexural and compressive strength values (Fig. 2), confirming the relation of this physical property with mechanical strength [26] within each series, higher UPV correspond to higher flexural and compressive strength values, even though for some samples, high errors in the mechanical strength values must be taken into account. For ghiara binders only, this trend can be confirmed also by peak stress values obtained from the Brazilian test and the most unstable fracture observed through DIC.

Specific weight, UPV and mechanical strength are also strictly related to the presence of soluble phases (e.g. salts) that are dissolved and leached out after exposure [51], increasing the total mass amount of the non-exposed samples.

Wetting and drying conditions at which geopolymer have been exposed can play dominant roles in controlling the moisture absorption/desorption isotherms and the formation of soluble phases. Carbonation of mobile alkalis from the pore solution leads to the formation of efflorescences and sub-efflorescences, sometimes accompanied by a reduction in mechanical strength. This induces a structural degradation due to the due to the decrease of the alkalinity of the aqueous solution present inside the pores [69].

For non-exposed samples, the graduality of the adsorption-desorption process over time may indicate that the materials themselves are still somehow reactive and not totally stable. In fact, water evaporation that occurs on the exterior of geopolymer specimens induces moisture transportation in the pore structure, which moves the free alkalis from the matrix to the surface where they can react with the atmospheric CO_2 forming efflorescences [44].

For exposed samples, DVS measurements clearly showed how the weathering process strongly influences the sorption-desorption properties of the materials, reducing the maxima EMC values to less than half of what is found for unexposed samples [51]. Looking at the EMC and RH% change over time, it can be observed that the materials after exposure have reached a higher degree of stability and are thus less reactive in presence of different relative amounts of moisture. On the other hand, from the hysteresis curves maxima, it can be inferred that the 35–55% RH, is the RH% interval to pay attention to when these materials are in use.

Among the identified salts, natron is the most commonly reported on building materials, while natrite is rarer. However, the lower winter temperature can have favoured its precipitation. The high solubility favoured the leaching out (rain) of the hydrated phase [51], while the high mobility of ions within the pores network can have been lowered by the decrease of the environmental temperature in winter. The effect of temperature on the behaviour of the anhydrous phase is particularly relevant and can lead to a quick precipitation of natrite.

As reported in Ref. [51], natron was mostly detected on unexposed materials and this is consistent with its instability at environmental conditions leading it to dissolve in its own crystal water at about 33 °C [70], a temperature easily reachable in Catania during the exposure period. In addition, Libowitzky and Giester [71] reported on the change of the carbonate group of natron from an ordered one at low temperature (110 K) to a partially disordered structure at environmental condition (295K), without any change of the space group symmetry. The presence of natron in the unexposed geopolymer samples, may explain their water sorption behaviour.

Variations in moisture sorption behaviour of unexposed and exposed binders and mortars reflect different mechanisms of carbonation, which is strongly dependent on the type of precursor (even though ghiara and ash are very similar in composition [52]), amount of binder formation, different diffusional and chemical mechanisms and the pore solution environment, CO_2 concentration in the external atmosphere, and relative humidity of the materials.

To summarize, specific weight, UPV, mechanical strength values, DVS and previous FTIR findings [51] are consistent for both series, namely.

- for GM series more efflorescences were found on the unexposed samples, leached after weathering, therefore, after exposure, UPV and specific weight decrease as a consequence of porosity increase, as well as mechanical performances get worse.
- for VM series, the behaviour is opposite, but still consistent for all the considered parameters and not significant for specific weight and tensile strength.

The opposite behavior of GM and VM series after weathering confirms a better response of volcanic-ash based geopolymers to the aging [51]. This could be explained because the alkali activation reaction continues over time, as long as the pore alkalinity solution remains high and the results is a better gel densification [72].

5. Conclusions

The innovative combination of ultrasound pulse velocity and dynamic vapour sorption applied to the study of naturally weathered geopolymers proved effective to study structural properties and the moisture sorption behaviour of these materials. The understanding of such properties is in turn fundamental to further develop formulations with improved performances in terms of durability in relation to the environmental conditions.

Weather-induced mechanisms of attack on geopolymer binders and mortars can be problematic under given circumstances and in some climatic conditions. The loss of alkalinity via leaching, carbonation or other mechanisms, is the primary cause of the material degradation, as clearly emerged in this work: the presence of salts can, for example, change the water sorption-desorption properties of materials.

All the data collected in this study on unexposed and exposed samples seem to converge towards confirming a better response of the volcanic ash-based geopolymers to the natural exposure to atmospheric agents in the Catania climate, representative of hot summer Mediterranean [73] zone, probably assisted by a better compaction of the matrix as the reaction proceeds. Ghiara-based products, instead, already showing some mixing difficulties during their preparation, are more affected by exposure conditions.

In conclusion, this work confirms that volcanic ash binders and mortars may actually find application as high performance advanced green materials in cultural heritage field, as demonstrated also by a recent preliminary test application to conservation works [74]. On the other hand, the author believe that a future development could be extended also to the construction sector, especially for pre-casted elements (such as tiles, bricks) in outdoor applications.

Declaration of competing interest

The authors declare that they have no known competing financial interests or personal relationships that could have appeared to influence the work reported in this paper.

Acknowledgements

This research is supported by Advanced Green Materials for Cultural Heritage (AGM for CuHe) (PNR fund with code: ARS01_00697; CUP E66C18000380005), SETI (PO FESR Sicilia; CUP G38118000960007) and Attraction and International Mobility (AIM1833071; CUP E66C18001310007) projects.

References

[1] C. Shi, B. Qu, J.L. Provis, Recent progress in low-carbon binders, Cement Concr. Res. 122 (2019) 227–250, https://doi.org/10.1016/j.cemconres.2019.05.009.
[2] A. Palomo, O. Maltseva, I. Garcia-Lodeiro, A. Fernández-Jiménez, Portland versus alkaline cement: continuity or clean break: "A key decision for global sustainability, Front. Chem. 9 (2021), https://doi.org/10.3389/FCHEM.2021.705475/FULL.
[3] T. Hanzlíček, M. Steinerová, P. Straka, I. Perná, P. Siegl, T. Švarcová, Reinforcement of the terracotta sculpture by geopolymer composite, Mater. Des. 30 (2009) 3229–3234, https://doi.org/10.1016/j.matdes.2008.12.015.
[4] K. Elert, E.S. Pardo, C. Rodriguez-Navarro, Alkaline activation as an alternative method for the consolidation of earthen architecture, J. Cult. Herit. 16 (2015) 461–469, https://doi.org/10.1016/j.culher.2014.09.012.
[5] S. Tamburini, M. Natali, E. Garbin, M. Panizza, M. Favaro, M.R. Valluzzi, Geopolymer matrix for fibre reinforced composites aimed at strengthening masonry structures, Construct. Build. Mater. 141 (2017) 542–552, https://doi.org/10.1016/j.conbuildmat.2017.03.017.
[6] M. Clausi, S.C. Tarantino, L.L. Magnani, M.P. Riccardi, C. Tedeschi, M. Zema, Metakaolin as a precursor of materials for applications in Cultural Heritage: geopolymer-based mortars with ornamental stone aggregates, Appl. Clay Sci. 132–133 (2016) 589–599, https://doi.org/10.1016/j.clay.2016.08.009.
[7] M. Clausi, M.P. Riccardi, M. Zema, S. Chiara Tarantino, Interaction of Metakaolin-Based Geopolymers with Natural and Artificial Stones and Implications on Their Use in Cultural Heritage Internationational Entrepreneurship and Global Value Chains in the Circular Economy View Project, 2016. www.ijcs.uaic.ro.
[8] R. Occhipinti, A. Stroscio, C. Finocchiaro, M. Fugazzotto, C. Leonelli, M. José Lo Faro, B. Megna, G. Barone, P. Mazzoleni, Alkali activated materials using pumice from the Aeolian Islands (Sicily, Italy) and their potentiality for cultural heritage applications: preliminary study, Construct. Build. Mater. 259 (2020), 120391, https://doi.org/10.1016/j.conbuildmat.2020.120391.
[9] F. Pacheco-Torgal, J. Labrincha, C. Leonelli, A. Palomo, P. Chindaprasit, Handbook of Alkali-Activated Cements, Mortars and Concretes, Woodhead Publishing, 2014. http://125.234.102.150:8080/dspace/handle/DNULIB_52011/8031.
[10] J.L. Provis, J.S.J. van Deventer, Alkali Activated Materials: State-Of-The-Art Report, RILEM TC 224-AAM, 2014, https://doi.org/10.1007/978-94-007-7672-2.
[11] J.L. Provis, Alkali-activated materials, Cement Concr. Res. 114 (2018) 40–48, https://doi.org/10.1016/j.cemconres.2017.02.009.
[12] J.G.S. Van Jaarsveld, J.S.J. Van Deventer, G.C. Lukey, The characterisation of source materials in fly ash-based geopolymers, n.d. www.elsevier.com/locate/matlet.
[13] M. Torres-Carrasco, F. Puertas, Waste glass in the geopolymer preparation. Mechanical and microstructural characterisation, J. Clean. Prod. 90 (2015) 397–408, https://doi.org/10.1016/j.jclepro.2014.11.074.
[14] R. Occhipinti, A.M. Fernández-Jiménez, A. Palomo, S.C. Tarantino, M. Zema, Sulfate-bearing clay and Pietra Serena sludge: raw materials for the development of alkali activated binders, Construct. Build. Mater. 301 (2021), 124030, https://doi.org/10.1016/j.conbuildmat.2021.124030.
[15] L.S. Wong, Durability performance of geopolymer concrete: a review, Polymers 14 (2022) 868, https://doi.org/10.3390/polym14050868.
[16] A.S. Noori, K.M. Oweed, R.M. Raouf, M.A. Abdulrehman, The relation between destructive and non-destructive tests of geopolymer concrete, Mater. Today Proc. 42 (2021) 2125–2133, https://doi.org/10.1016/j.matpr.2020.12.296.
[17] J. Shi, B. Liu, Y. Liu, E. Wang, Z. He, H. Xu, X. Ren, Preparation and characterization of lightweight aggregate foamed geopolymer concretes aerated using hydrogen peroxide, Construct. Build. Mater. 256 (2020), 119442, https://doi.org/10.1016/j.conbuildmat.2020.119442.
[18] M.P. Sáez-Pérez, M. Brümmer, J.A. Durán-Suárez, Effect of the state of conservation of the hemp used in geopolymer and hydraulic lime concretes, Construct. Build. Mater. 285 (2021), 122853, https://doi.org/10.1016/j.conbuildmat.2021.122853.
[19] A. Erfanimanesh, M.K. Sharbatdar, Mechanical and microstructural characteristics of geopolymer paste, mortar, and concrete containing local zeolite and slag activated by sodium carbonate, J. Build. Eng. 32 (2020), 101781, https://doi.org/10.1016/j.jobe.2020.101781.
[20] O. Baron, J, La durabilite des betons, COLLECTION, PRESSES DE L'ECOLE NATIONALE DES PONTS ET CHAUSSEES, 1992.
[21] L.P. Martin, D. Dadon, M. Rosen, Evaluation of ultrasonically determined elasticity-porosity relations in zinc oxide, J. Am. Ceram. Soc. 79 (1996) 1281–1289, https://doi.org/10.1111/j.1151-2916.1996.tb08585.x.
[22] D.G. Aggelis, T. Shiotani, Repair evaluation of concrete cracks using surface and through-transmission wave measurements, Cem. Concr. Compos. 29 (2007) 700–711, https://doi.org/10.1016/j.cemconcomp.2007.05.001.
[23] R. Jones, Surface wave technique for measuring the elastic properties and thickness of roads: theoretical development, Br. J. Appl. Phys. 13 (1962) 21–29, https://doi.org/10.1088/0508-3443/13/1/306.
[24] BS 1881-203-1986 – TESTING CONCRETE – Recommendations for Measurement of Velocity of Ultrasonicpulses Velocity, 1986.
[25] J.H. Bungey, M.G. Grantham, Testing of Concrete in Structures, CRC Press, 2006, https://doi.org/10.1201/9781482264685.
[26] B.S. Al-Nu'man, B.R. Aziz, S.A. Abdulla, S.E. Khaleel, Effect of aggregate content on the concrete compressive strength - ultrasonic pulse velocity relationship, Am. J. Civ. Eng. Architect. 4 (2017) 1–5, https://doi.org/10.12691/ajcea-4-1-1.
[27] Y. Zhang, O. Abraham, F. Grondin, A. Loukili, V. Tournat, A. Le Duff, B. Lascoup, O. Durand, Study of stress-induced velocity variation in concrete under direct tensile force and monitoring of the damage level by using thermally-compensated Coda Wave Interferometry, Ultrasonics 52 (2012) 1038–1045, https://doi.org/10.1016/j.ultras.2012.08.011.
[28] M. Kaya, F. Köksal, Effect of cement additive on physical and mechanical properties of high calcium fly ash geopolymer mortars, Struct. Concr. 22 (2021), https://doi.org/10.1002/suco.202000235.
[29] Y. Berthaud, Damage measurements in concrete via an ultrasonic technique. Part I experiment, Cement Concr. Res. 21 (1991) 73–82, https://doi.org/10.1016/0008-8846(91)90033-E.
[30] H. Aldeeky, O. Al Hattamleh, Prediction of engineering properties of basalt rock in Jordan using ultrasonic pulse velocity test, Geotech. Geol. Eng. 36 (2018) 3511–3525, https://doi.org/10.1007/S10706-018-0551-6/TABLES/8.
[31] J.A. Hudson, E.T. Brown, F. Rummel, The controlled failure of rock discs and rings loaded in diametral compression, Int. J. Rock Mech. Min. Sci. Geomech. Abstr. 9 (1972) 241–248, https://doi.org/10.1016/0148-9062(72)90025-3.
[32] Y.Y.G.X. Yu, J. Y, Questioning the validity of the Brazilian test for determining tensile strength of rocks, Rock Mech Eng 24 (7) (2005) 1150–1157.
[33] M. Mellor, I. Hawkes, Measurement of tensile strength by diametral compression of discs and annuli, Eng. Geol. 5 (1971) 173–225, https://doi.org/10.1016/0013-7952(71)90001-9.
[34] G.E. Andreev, A review of the Brazilian test for rock tensile strength determination. Part I: calculation formula, Min. Sci. Technol. 13 (1991) 445–456, https://doi.org/10.1016/0167-9031(91)91006-4.
[35] G.E. Andreev, A review of the Brazilian test for rock tensile strength determination. Part II: contact conditions, Min. Sci. Technol. 13 (1991) 457–465, https://doi.org/10.1016/0167-9031(91)91035-G.
[36] D. Li, L.N.Y. Wong, The Brazilian disc test for rock mechanics applications: review and new insights, Rock Mech. Rock Eng. 46 (2013) 269–287, https://doi.org/10.1007/s00603-012-0257-7.
[37] C. Johnstone, C. Ruiz, Dynamic testing of ceramics under tensile stress, Int. J. Solid Struct. 32 (1995) 2647–2656, https://doi.org/10.1016/0020-7683(94)00287-7.
[38] Z. Zhou, X. Li, Y. Zou, Y. Jiang, G. Li, Dynamic Brazilian tests of granite under coupled static and dynamic loads, Rock Mech. Rock Eng. 47 (2014) 495–505, https://doi.org/10.1007/s00603-013-0441-4.
[39] J.R.C. Proveti, G. Michot, The Brazilian test: a tool for measuring the toughness of a material and its brittle to ductile transition, Int. J. Fract. 139 (2006) 455–460, https://doi.org/10.1007/s10704-006-0067-6.
[40] W.H. Peters, W.F. Ranson, Digital imaging techniques in experimental stress analysis, Opt. Eng. 21 (1982), https://doi.org/10.1117/12.7972925.
[41] Z. Zhou, P. Chen, F. Huang, S. Liu, Experimental study on the micromechanical behavior of a PBX simulant using SEM and digital image correlation method, Opt Laser. Eng. 49 (2011) 366–370, https://doi.org/10.1016/j.optlaseng.2010.11.001.
[42] N. Zhang, A. Hedayat, H.G. Bolaños Sosa, N. Tupa, I. Yanqui Morales, R.S. Canahua Loza, Crack evolution in the Brazilian disks of the mine tailings-based geopolymers measured from digital image correlations: an experimental investigation considering the effects of class F fly ash additions, Ceram. Int. 47 (2021) 32382–32396, https://doi.org/10.1016/j.ceramint.2021.08.138.
[43] K. Arnold, A. Zehnder, Monitoring wall paintings affected by soluble salts, in: The Conservation of Wall Paintings, in: Proc. A Symp. Organ. by Court, Inst. Art Getty Conserv. Inst., 1987, pp. 103–135.
[44] S. Zhou, S. Zhou, J. Zhang, X. Tan, D. Chen, Relationship between moisture transportation, efflorescence and structure degradation in fly ash/slag geopolymer, Materials 13 (2020) 5550, https://doi.org/10.3390/ma13235550.
[45] Z. Zhang, J.L. Provis, A. Reid, H. Wang, Fly ash-based geopolymers: the relationship between composition, pore structure and efflorescence, Cement Concr. Res. 64 (2014) 30–41, https://doi.org/10.1016/j.cemconres.2014.06.004.
[46] E. Najafi Kani, A. Allahverdi, J.L. Provis, Efflorescence control in geopolymer binders based on natural pozzolan, Cem. Concr. Compos. 34 (2012) 25–33, https://doi.org/10.1016/j.cemconcomp.2011.07.007.
[47] A.J.J. van der Z, H.J.H.B.A. Taher, T. Arends, Measuring water sorption isotherm of mortar containing chloride, in: XIII Int. Conf. Durab, . Build. Mater. Components, 2014, pp. 1093–1100.
[48] H. Garbalińska, M. Bochenek, M. Stasiak, Experimental and modeling investigations on the water sorption behaviors of autoclaved aerated concrete, Materials 14 (2021) 6235, https://doi.org/10.3390/ma14216235.
[49] M.C. Caggiani, A. Coccato, G. Barone, C. Finocchiaro, M. Fugazzotto, G. Lanzafame, R. Occhipinti, A. Stroscio, P. Mazzoleni, Raman spectroscopy potentiality in the study of geopolymers reaction degree, J. Raman Spectrosc. (2021), jrs.6167, https://doi.org/10.1002/jrs.6167.
[50] G. Barone, M.C. Caggiani, A. Coccato, C. Finocchiaro, M. Fugazzotto, G. Lanzafame, R. Occhipinti, A. Stroscio, P. Mazzoleni, Geopolymer production for conservation-restoration using Sicilian raw materials: feasibility studies, IOP Conf. Ser. Mater. Sci. Eng. 777 (2020), 012001, https://doi.org/10.1088/1757-899X/777/1/012001.

[51] R. Occhipinti, M.C. Caggiani, F. Andriulo, G. Barone, L. de Ferri, P. Mazzoleni, Effect of atmospheric exposure on alkali activated binders and mortars from Mt. Etna volcanic precursors, Mater. Lett. 315 (2022), 131940, https://doi.org/10.1016/j.matlet.2022.131940.
[52] C. Finocchiaro, G. Barone, P. Mazzoleni, C. Leonelli, A. Gharzouni, S. Rossignol, FT-IR study of early stages of alkali activated materials based on pyroclastic deposits (Mt. Etna, Sicily, Italy) using two different alkaline solutions, Construct. Build. Mater. 262 (2020), 120095, https://doi.org/10.1016/j.conbuildmat.2020.120095.
[53] L. de Ferri, C. Santagati, M. Catinoto, E. Tesser, E.M. di San Lio, G. Pojana, A multi-technique characterization study of building materials from the Exedra of S. Nicolò l'Arena in Catania (Italy), J. Build. Eng. 23 (2019) 377–387, https://doi.org/10.1016/j.jobe.2019.01.028.
[54] G. Lanzafame, M.C. Caggiani, C. Finocchiaro, G. Barone, C. Ferlito, L. Gigli, P. Mazzoleni, Multidisciplinary characterization of the "Ghiara" volcanic paleosoil (Mt. Etna volcano, Italy): petrologic characters and genetic model, Lithos 418–419 (2022), 106679, https://doi.org/10.1016/J.LITHOS.2022.106679.
[55] R. Occhipinti, A.M. Fernández-Jiménez, A. Palomo, S.C. Tarantino, M.P. Riccardi, M. Clausi, M. Zema, Effect of NaOH molarity on the formation of hybrid cements from sulfate-bearing clay and Pietra Serena sludge, Mater. Lett. 335 (2023), 133774, https://doi.org/10.1016/j.matlet.2022.133774.
[56] F. Lionetto, M. Frigione, Mechanical and natural durability properties of wood treated with a novel organic preservative/consolidant product, Mater. Des. 30 (2009) 3303–3307, https://doi.org/10.1016/j.matdes.2008.12.010.
[57] K. Zalegowski, Assessment of polymer concrete sample geometry effect on ultrasonic wave velocity and spectral characteristics, Materials 14 (2021) 7200, https://doi.org/10.3390/ma14237200.
[58] C. Fairhurst, On the validity of the 'Brazilian' test for brittle materials, Int. J. Rock Mech. Min. Sci. Geomech. Abstr. 1 (1964) 535–546, https://doi.org/10.1016/0148-9062(64)90060-9.
[59] N. Volkova, H. Hansson, L. Ljunggren, Thermally decarboxylated sodium bicarbonate: interactions with water vapour, calorimetric study, J. Pharm. Anal. 3 (2013) 193–199, https://doi.org/10.1016/J.JPHA.2012.12.003.
[60] D. Bionda, Modelling Indoor Climate and Salt Behaviour in Historical Buildings: a Case Study, 2006.
[61] Herbert Pöllmann, Syntheses, properties and solid solution of ternary lamellar calcium aluminate hydroxi salts (AFm-phases) containing SO42, CO32 and OH, Neues Jahrbuch Mineral. Abhand. 182 (2006) 173–181, https://doi.org/10.1127/0077-7757/2006/0042.
[62] B. Libby, P.A. Monson, Adsorption/desorption hysteresis in inkbottle pores: a density functional theory and Monte Carlo simulation study, Langmuir 20 (2004) 4289–4294, https://doi.org/10.1021/la036100a.
[63] Z. Wu, H.S. Wong, N.R. Buenfeld, Transport properties of concrete after drying-wetting regimes to elucidate the effects of moisture content, hysteresis and microcracking, Cement Concr. Res. 98 (2017) 136–154, https://doi.org/10.1016/j.cemconres.2017.04.006.
[64] S. Sheokand, S.R. Modi, A.K. Bansal, Dynamic vapor sorption as a tool for characterization and quantification of amorphous content in predominantly crystalline materials, J. Pharmaceut. Sci. 103 (2014) 3364–3376, https://doi.org/10.1002/jps.24160.
[65] E. Vasanelli, D. Colangiuli, A. Calia, M. Sileo, M.A. Aiello, Ultrasonic pulse velocity for the evaluation of physical and mechanical properties of a highly porous building limestone, Ultrasonics 60 (2015) 33–40, https://doi.org/10.1016/j.ultras.2015.02.010.
[66] M. Benaicha, O. Jalbaud, A. Hafidi Alaoui, Y. Burtschell, Correlation between the mechanical behavior and the ultrasonic velocity of fiber-reinforced concrete, Construct. Build. Mater. 101 (2015) 702–709, https://doi.org/10.1016/j.conbuildmat.2015.10.047.
[67] L. Lin, Yiching, Kuo Shih-Fang, Chiamen Hsiao, Chao-Peng, Investigation of pulse velocity-strength relationship of hardened concrete - ProQuest, ACI Mater. J. 104 (2007) 344–350.
[68] S.A. Abo-Qudais, Effect of concrete mixing parameters on propagation of ultrasonic waves, Construct. Build. Mater. 19 (2005) 257–263, https://doi.org/10.1016/j.conbuildmat.2004.07.022.
[69] Z. Zhang, J.L. Provis, X. Ma, A. Reid, H. Wang, Efflorescence and subflorescence induced microstructural and mechanical evolution in fly ash-based geopolymers, Cem. Concr. Compos. 92 (2018) 165–177, https://doi.org/10.1016/j.cemconcomp.2018.06.010.
[70] C. Bu, G. Rodriguez Lopez, C.A. Dukes, L.A. McFadden, J.-Y. Li, O. Ruesch, Stability of hydrated carbonates on Ceres, Icarus 320 (2019) 136–149, https://doi.org/10.1016/j.icarus.2017.12.036.
[71] E. Libowitzky, G. Giester, Washing soda (natron), Na 2 CO 3 *10H 2 O, revised: crystal structures at low and ambient temperatures, Mineral. Petrol. 77 (2003) 177–195, https://doi.org/10.1007/s00710-002-0215-2.
[72] S.A. Bernal, J.L. Provis, Durability of alkali-activated materials: progress and perspectives, J. Am. Ceram. Soc. (2014), https://doi.org/10.1111/jace.12831.
[73] H.E. Beck, N.E. Zimmermann, T.R. McVicar, N. Vergopolan, A. Berg, E.F. Wood, Present and future Köppen-Geiger climate classification maps at 1-km resolution, Sci. Data 5 (2018), 180214, https://doi.org/10.1038/sdata.2018.214.
[74] M. Fugazzotto, R. Occhipinti, M.C. Caggiani, A. Coccato, C. Finocchiaro, G. Lanzafame, P. Mazzoleni, G. Nucatolo, G. Piacenti, S. Starinieri, A. Stroscio, G. Barone, Restoration feasibility study by using alkali activated mortars based on Mt. Etna volcanic ash: the case study of Monreale Cathedral (Palermo, Italy), Mater. Lett. 333 (2023), 133626, https://doi.org/10.1016/j.matlet.2022.133626.